# HIGH ACCURACY INDOOR LOCALIZATION: A WIFI-BASED APPROACH

*Chen Chen*[⋆†], *Yan Chen*[⋆†], *Hung-Quoc Lai*[†], *Yi Han*[⋆†], *and K.J. Ray Liu*[⋆†]

[⋆] University of Maryland, College Park, MD 20742, USA
[†] Origin Wireless, 223 Newbury Street Boston, MA 02116, USA
[⋆] School of Electronic Engineering, University of Electronic Science and Technology of China

## ABSTRACT

Indoor positioning systems (IPS) based on Wi-Fi signals are gaining popularity recently. IPS based on Received Signal Strength Indicator (RSSI) could only achieve a precision of several meters due to the strong temporal and spatial variation of indoor environment. On the other hand, IPS based on Channel State Information (CSI) drive the precision into the sub-meter regime with several access points (AP). However, the performance degrades with fewer APs mainly due to the limit of bandwidth. In this paper, we propose a Wi-Fi-based time-reversal indoor positioning system (WiFi-TRIPS) using the location-specific fingerprints generated by CSIs with a total bandwidth of 1 GHz. WiFi-TRIPS consists of an offline phase and an online phase. In the offline phase, CSIs are collected in different 10 MHz bands from each location-of-interest and the timing and frequency synchronization errors are compensated. We perform a bandwidth concatenation to combine CSIs in different bands into a single fingerprint of 1 GHz. In the online phase, we evaluate the time-reversal resonating strength using the fingerprint from an unknown location and those in the database for location estimation. Extensive experiment results demonstrate a perfect $5cm$ precision in an $20cm \times 70cm$ area in a non-line-of-sight office environment with one link measurement.

***Index Terms***— WiFi, Localization, Channel State Information, Time-reversal Resonating Strength

## 1. INTRODUCTION

Wireless indoor positioning systems (IPS) have become popular recently. It spawns a lot of location-based applications, such as personalized advertisement in a grocery store, tourist guidance in a museum, and goods localization in a warehouse, to name a few.

Speaking of outdoor localization systems, Global Positioning System (GPS) has provided routes to millions of drivers for years. However, the GPS signal could be too weak when it comes to indoor localization: the blocking of concrete walls and floors severely attenuates the signal. On the other hand, the precision in the order of tens of meters is far from satisfactory for indoor applications.

Realizing these drawbacks, many researchers and companies harness the ubiquitous wireless local area networks (WLAN) powered by WiFi technology. Received Signal Strength Indicator (RSSI) is a MAC layer, coarse-grained information available in mainstream wireless network interface controllers (NIC) [1]. Thus, RSSI-based IPS have been well studied. In [2], the authors presented Horus which utilized the RSSIs reported by access points (AP) to build a radio map in the offline phase. In the online phase, the RSSIs from nearby APs are measured and matched to the radio map, resulting in a probabilistic location estimation. It achieved an average accuracy of $2m$. Other RSSI-based systems such as RADAR [3] and MultiLoc [4] could achieve $3 \sim 5m$ and $2.7m$ in mean accuracy. However, RSSI-based schemes suffer in an environment with strong non-line-of-sight (NLOS) condition.

The precision could be further driven into sub-meter regime using channel state information (CSI), a physical layer, fine-grained information at the receiver. Orthogonal-Frequency-Division-Multiplexing (OFDM) is one of the baseband technique in WLANs, where CSIs are estimated from the long training preambles (LTP) on subcarrier level in frequency domain. In [5], the authors proposed the PinLoc system. They performed a wardriving to obtain CSIs from APs in an area of $1m \times 1m$ in the offline phase. In the online phase, the similarity of the CSIs from multiple nearby APs and those in the offline phase was calculated for localization, resulting in $89\%$ mean accuracy and $6\%$ false positives. In [6], the authors proposed FIFS using the summation of power across subcarriers in CSI to achieve $0.60m$ median accuracy.

However, most IPS systems cannot achieve a centimeter accuracy, particularly in an environment with scarce APs and/or strong NLOS condition. It is mainly due to the limited bandwidth of 10 or 20 MHz in 802.11a/g/p WLANs, which is not sufficient to resolve enough independent multipaths and consequently, introduces ambiguity into the CSIs. In light of this, Wu et al. proposed Time-reversal (TR) indoor positioning system (TRIPS) in [7] using a much larger bandwidth of 125 MHz on the 5.4 GHz band. It utilized the super-resolution spatial-temporal focusing effect of TR [8] in a rich-scattering environment. It achieved a perfect $10cm$ localization accu-

racy within a $0.9m \times 1m$ area-of-interest in a NLOS environment.

Inspired by TRIPS, we implement the WiFi-based TRIPS (WiFi-TRIPS). We extend from the 802.11a/g/p baseband processor developed in [9] on Universal Software Radio Peripheral (USRP) [10] in the framework of GNU Radio [11]. Instead of the pilot-assisted channel estimator in [9], we use the two LTPs defined in 802.11a/g/p for channel estimation. To obtain CSIs from a much wider bandwidth, we perform a frequency sweeping of 1 GHz from 4.9 GHz to 5.9 GHz on a single link.

Similar to TRIPS, WiFi-TRIPS consists of two phases. In the offline phase, WiFi-TRIPS collect CSIs from location-of-interest which are stored into the database. Three synchronization errors might exist in the CSIs: (i) Symbol Timing Offset (STO) caused by the misalignment between the correct starting point of the frame and the estimated starting point (ii) Carrier Frequency Offset (CFO) caused by the difference between the two oscillators at the transmitter (TX) for up-conversion and the receiver (RX) for down-conversion (iii) Sampling Frequency Offset (SFO) caused by the difference in the sampling frequency between TX and RX. In order to combat the residual timing and frequency synchronization error, we propose an algorihm for compensation. With bandwidth concatenation, we combine the sanitized CSIs from different bands into one fingerprint. In the online phase, the TR resonating strength is calculated for location estimation. We perform extensive experiments with a unit distance of $5cm$ to demonstrate the centimeter-level accuracy of WiFi-TRIPS in a typical office environment during day time. We achieve a perfect localization accuracy in an area of $20cm \times 70cm$ using only one link measurement of CSI.

## 2. SYSTEM ARCHITECTURE

The system architecture of the WiFi-TRIPS is shown in Fig. 1. The transmitter USRP (TX-USRP) upsamples the baseband signal, followed by low-pass filtering and digital-to-analog conversion. Then, the upsampled signal is up converted to the center frequency and transmitted over the air. The receiver USRP (RX-USRP) down converts the signal to zero center frequency, performs low-pass filtering and analog-to-digital conversion, followed by downsampling. The channel estimation block at the receiver could obtain the CSI for each frame. To enhance the quality of CSIs, we only keep those with correctly decoded data frames. The two USRPs jump to the next center frequency after enough CSIs are collected at the present center frequency.

## 3. PROPOSED ALGORITHM

We label each geographical location with a coordinate $p_\ell$. For convenience, we refer to this location as *logical location* $\ell$.

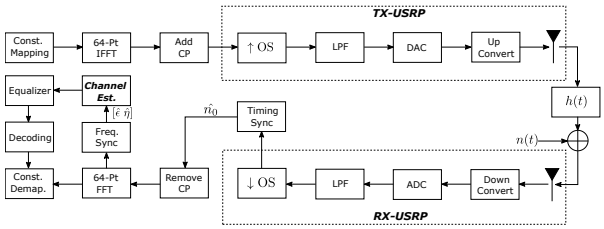


**Fig. 1**. Architecture of the measurement platform

Since the mapping from the geographical location to the logical location is one-to-one, we transform the estimation of geographical locations into estimation of logical locations.

Assume that for logical location $\ell$ and frequency band $f_d$, $N_{\ell,f_d}$ CSIs are measured from the first and second LTPs, written as

$$\mathbb{H}_i\left[\ell, f_d\right] = \left[\mathbf{H}_{i,1}^T[\ell, f_d] \cdots \mathbf{H}_{i,m}^T[\ell, f_d] \cdots \mathbf{H}_{i,N_{\ell,f_d}}^T[\ell, f_d]\right]^T, \tag{1}$$

where $m$ is the realization index, $i \in \{1, 2\}$ as the LTP index, and $\mathbf{H}_{i,m}[\ell, f_d] = \left[\hat{H}_{i,m}^{u_1}[\ell, f_d] \cdots \hat{H}_{i,m}^{u_k}[\ell, f_d] \cdots \hat{H}_{i,m}^{u_K}[\ell, f_d]\right]$ where $u_k$ denotes the subcarrier index of the $k$-th usable subcarrier, and $K$ the total number of usable subcarriers. The channel estimation $\hat{H}_{i,m}^{u_k}[\ell, f_d]$ can be written as

$$\hat{H}_{i,m}^{u_k}[\ell, f_d] = \frac{Y_{i,m}^{u_k}[\ell, f_d]}{X_{i,u_k}}, \tag{2}$$

where $Y_{i,m}^{u_k}[\ell, f_d]$ is the $m$-th received symbol in frequency domain on the $k$-th subcarrier, and $X_{i,u_k}$ is the transmitted symbol of the $i$-th LTP on the $k$-th subcarrier.

### 3.1. Effect of CFO, SFO, and STO on CSI

In presence of CFO $\epsilon$, SFO $\eta$, and STO $\Delta n_0$, $\hat{H}_{i,m}^{u_k}[\ell, f_d]$ in Equ. (2) can be written as [12, 13]

$$\begin{aligned}\hat{H}_{i,m}^{u_k}[\ell, f_d] &= H_{i,m}^{u_k}[\ell, f_d] e^{j2\pi\Delta n_0 \frac{u_k}{N}} \\ & e^{j\pi\phi_{u_k}} e^{j2\pi\frac{iN_s+N_g}{N}\phi_{u_k}} \mathrm{sinc}\left(\pi\phi_{u_k}\right) + n_{i,m}^{u_k}[\ell, f_d],\end{aligned} \tag{3}$$

where $\phi_{u_k} = \epsilon + \eta u_k$, $N$ the size of Fast Fourier Transform (FFT), $N_g$ the length of cyclic prefix, $N_s = N + N_g$, and $n_{i,m}^{u_k}[\ell, f_d]$ the estimation noise.

In the following, we introduce the two phases in the proposed algorithm.

### 3.2. Offline Phase

#### *3.2.1. Residual CFO/SFO Estimation and Compensation*

To estimate the residual CFO and SFO from the channel estimation, we could use [14]

$$\begin{aligned}\Omega_m^{u_k}[\ell, f_d] &= \left[\hat{H}_{1,m}^{u_k}[\ell, f_d]\right]^* \times \hat{H}_{2,m}^{u_k}[\ell, f_d] \\ &= e^{j2\pi\frac{N_s}{N}\phi_{u_k}} |H_{1,m}^{u_k}[\ell, f_d]|^2 \mathrm{sinc}^2\left(\pi\phi_{u_k}\right) + \psi_m^{u_k}[\ell, f_d],\end{aligned} \tag{4}$$

where $\mathrm{sinc}^2(\pi\phi_k) \approx 1$ since $\pi\phi_{u_k}$ is small, and $\psi_m^{u_k}[\ell, f_d]$ is the cross terms. Therefore, $\phi_{u_k}$ can be estimated by

$$\hat{\phi}_{u_k} = \measuredangle\left[\Omega_m^{u_k}[\ell, f_d]\right], \tag{5}$$

where $\measuredangle[X]$ is the angle of $X$. Compensating $\hat{\phi}_{u_k}$ gives

$$\tilde{H}_{i,m}^{u_k}[\ell, f_d] = \hat{H}_{i,m}^{u_k}[\ell, f_d] e^{-j\pi\hat{\phi_{u_k}}} e^{-j2\pi\frac{N_g+(i-1)N_s}{N}\hat{\phi_{u_k}}} \tag{6}$$

Substituting Equ. (6) into Equ. (1) and writing the updated $\mathbb{H}_i[\ell, f_d]$ in Equ. (1) as $\tilde{\mathbb{H}}_i[\ell, f_d]$, we take the average of $\tilde{\mathbb{H}}_1[\ell, f_d]$ and $\tilde{\mathbb{H}}_2[\ell, f_d]$ as $\tilde{\mathbb{H}}[\ell, f_d] = \frac{\tilde{\mathbb{H}}_1[\ell, f_d]+\tilde{\mathbb{H}}_2[\ell, f_d]}{2}$.

#### 3.2.2. STO Estimation and Compensation

After removing the residual CFO and SFO, the STO still remains to be compensated. Write

$$\tilde{\mathbb{H}}[\ell, f_d] = \left[\tilde{\mathbf{H}}_1^T[\ell, f_d] \cdots \tilde{\mathbf{H}}_m^T[\ell, f_d] \cdots \tilde{\mathbf{H}}_{N_{\ell,f_d}}^T[\ell, f_d]\right]^T, \tag{7}$$

where $\tilde{\mathbf{H}}_m[\ell, f_d] = \left[\tilde{H}_m^{u_1}[\ell, f_d] \cdots \tilde{H}_m^{u_k}[\ell, f_d] \cdots \tilde{H}_m^{u_K}[\ell, f_d]\right]$ is the CSI vector for the $m$-th realization on usable subcarriers after CFO/SFO correction. Denote $A_m^{u_k}[\ell, f_d] = \measuredangle\left\{\tilde{H}_m^{u_k}[\ell, f_d]\right\}$ as the angle of $\tilde{H}_m^{u_k}[\ell, f_d]$, we take a phase unwrapping on all $A_m^{u_k}[\ell, f_d]$, which gives $A_m^{'u_k}[\ell, f_d]$. The slope of $A_m^{'u_k}[\ell, f_d]$ is linear with STO if we disregard the noise and interference. To estimate the slope, we use a linear square fitting on $A_m^{'u_k}[\ell, f_d]$, leading to

$$\widehat{\Delta n_0} = \frac{N\sum_{k=1}^{K}\left[(u_k - \overline{u})\right]\left[A_m^{'u_k}[\ell, f_d] - \overline{A}\right]}{2\pi\sum_{k=1}^{K}\left[u_k - \overline{u}\right]^2}, \tag{8}$$

where $\overline{u} = \frac{\sum_{k=1}^{K} u_k}{K}$ and $\overline{A} = \frac{\sum_{k=1}^{K} A_m^{'u_k}[\ell, f_d]}{K}$. Therefore, $\tilde{H}_m^{u_k}[\ell, f_d]$ is corrected as

$$\check{H}_m^{u_k}[\ell, f_d] = \tilde{H}_m^{u_k}[\ell, f_d] e^{-ju_k\widehat{\Delta n_0}\frac{2\pi}{N}}. \tag{9}$$

#### 3.2.3. Formulating the Localization Fingerprint

Write the CSI matrix after STO compensation as

$$\check{\mathbb{H}}[\ell, f_d] = \left[\check{\mathbf{H}}_1^T[\ell, f_d] \cdots \check{\mathbf{H}}_m^T[\ell, f_d] \cdots \check{\mathbf{H}}_{N_{\ell,f_d}}^T[\ell, f_d]\right]^T, \tag{10}$$

we could formulate a localization fingerprint at location $\ell$ and frequency band $f_d$ as

$$\mathbf{S}[\ell, f_d] = \frac{1}{N_{\ell,f_d}}\sum_{m=1}^{N_{\ell,f_d}} \check{\mathbf{H}}_m[\ell, f_d] \cdot \mathbf{W}_m, \tag{11}$$

where $\cdot$ stands for the dot product between two vectors. $\mathbf{W}_m$ is a $K$-dimension vector given by

$$\mathbf{W}_m = \begin{bmatrix} w_m[\ell, f_d] & w_m[\ell, f_d] & \cdots & w_m[\ell, f_d] \end{bmatrix}, \tag{12}$$

where $w_m[\ell, f_d] = e^{-j\measuredangle\left[\check{H}_m^{u_1}[\ell, f_d]\right]}$.

After bandwidth concatenation, the localization fingerprint $\mathbf{G}[\ell]$ can be written as

$$\mathbf{G}[\ell] = \begin{bmatrix} \mathbf{S}[\ell, f_1] & \mathbf{S}[\ell, f_2] & \cdots & \mathbf{S}[\ell, f_D] \end{bmatrix}, \tag{13}$$

where $D$ is the total number of frequency bands. The fingerprints for all locations $\ell = 1, 2, \cdots, L$ are calculated and stored into the database.

### 3.3. Online Phase

#### 3.3.1. Processing the CSIs

In this step, we repeat the procedures in the offline phase on the CSIs collected from a location-of-interest to correct the synchronization issues and combine the CSIs into the location fingerprint.

#### 3.3.2. Localization by Calculating Resonating Strength

For the location fingerprint $\mathbf{G}[\ell']$ from a location-of-interest $\ell'$, the resonating strength is calculated as Equ. (14),

$$\Phi[\ell, \ell'] = \left|\frac{\mathbf{G}[\ell]\mathbf{G}[\ell']^\dagger}{||\mathbf{G}[\ell]||_2||\mathbf{G}[\ell']||_2}\right|^2, \tag{14}$$

where $\dagger$ stands for transpose and conjugate, and $||\mathbf{X}||_2$ the $\mathcal{L}2$ norm of vector $\mathbf{X}$. When $\ell = \ell'$, we have $\Phi[\ell, \ell'] = 1$. The estimated location $\hat{\ell}'$ is given as

$$\hat{\ell}' = \begin{cases} \arg\max_{\ell^*}\Phi[\ell^*, \ell'] & , \text{ if } \max_{\ell^*}\Phi[\ell^*, \ell'] \geq \Gamma \\ 0 & , \max_{\ell^*}\Phi[\ell^*, \ell'] < \Gamma \end{cases} \tag{15}$$

where $\ell^* = 1, 2, \cdots, L$ and $\Gamma$ is the threshold. When $\hat{\ell}' = 0$, we cannot achieve localization given $\mathbf{G}[\ell']$. It can be proved that Equ. (14) is the frequency domain expression of the time-reversal resonating strength defined in [7]. In this sense, we are calculating the resonating strength virtually.

## 4. EXPERIMENT RESULTS

The experiments are performed in an office environment during day time. The two USRPs are placed on the wooden architecture as shown in Fig. 2, with a unit distance of $5cm$ horizontally and vertically.

We use 30 dB gain at TX-USRP and 15 dB gain at the RX-USRP. RX-USRP locates on the wooden structure. The total number of subcarriers is 64, with 52 usable subcarriers of index $\{-26, -25, \cdots, -1, 1, \cdots, 25, 26\}$. The length of cyclic prefix is 16 with FFT size 64. The distance between the transmitter and receiver is 10 feet with a concrete wall in the middle.

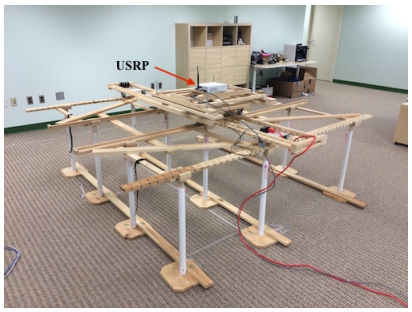


**Fig. 2**. The wooden architecture for measurements

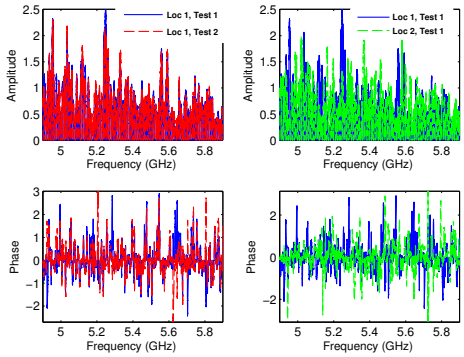


**Fig. 3**. 1 GHz fingerprints at two locations

The bandwidth is 10 MHz. To fill the missing null subcarriers in WiFi, we overlap the band between two consecutive frequency measurement: both USRPs increment the center frequency by 8.28125 MHz. We measure 124 frequency bands from 4.8909 GHz to 5.9091 GHz. The band $4.9 \sim 5.9$ GHz is chosen to formulate the localization fingerprint.

We measure a total of 75 locations in an area of $20cm \times 70cm$ located on a rectangular grid. The unit distance is $5cm$. For each location, we generate two fingerprints: the fingerprint associated with the first measurement is stored into database in the offline phase, while the second fingerprint is regarded as generated from the location-of-interest in the online phase for location estimation.

In Fig. 3, we show the amplitudes and phases of the fingerprints at location 1 and location 2 separated by $5cm$. Obviously, the similarity between two fingerprints at the same location are much higher than that between two different locations.

In Fig. 4, we show the confusion matrix $\Phi$ under bandwidths $20, 120, 250, 500, 1000$ MHz using Equ. (14). Also, we demonstrate the mean of the diagonal elements ($\mu_{\text{diag}}$), mean of the off-diagonal elements ($\mu_{\text{offdiag}}$), the difference between $\mu_{\text{diag}}$ and $\mu_{\text{offdiag}}$, and value of $\Gamma$ such that we could achieve $100\%$ detection rate with $0\%$ false alarm rate, under bandwidths from 10 MHz to 1000 MHz. For convenience of demonstration, if we fail to find such a $\Gamma$, we set $\Gamma = 0$.

We conclude that (i) The resonating strength at the same location is much higher than that from different locations (ii) Larger bandwidth in general improves the performance. However, the fingerprint could be impaired by the imperfect corrections of residual STO/CFO/SFO. It is possible that with a large bandwidth, we cannot find $\Gamma$ to get $100\%$ detection rate with $0\%$ false alarm rate (iii) $\Gamma = 0.9380$ when we only use 20 MHz bandwidth, predicting a poor performance when dynamics exist in the environment (iv) When bandwidth increases, both of $\mu_{\text{diag}}$ and $\mu_{\text{offdiag}}$ decreases. The gap between them is maximized when bandwidth equals 390 MHz. The performance improvement with larger bandwidth is more distinct when bandwidth falls in the range of $90 \sim 150$ MHz. Also, we achieve perfect localization performance in the range of $90 \sim 150$ MHz. (v) Based on our more recent results, the results can be generalized to a larger indoor space. Because of the rich scattering characteristic inherent in the indoor environment, it is highly unlikely to pinpoint a spatial position with high correlation with the fingerprint formulated across a wide range of frequency bands.

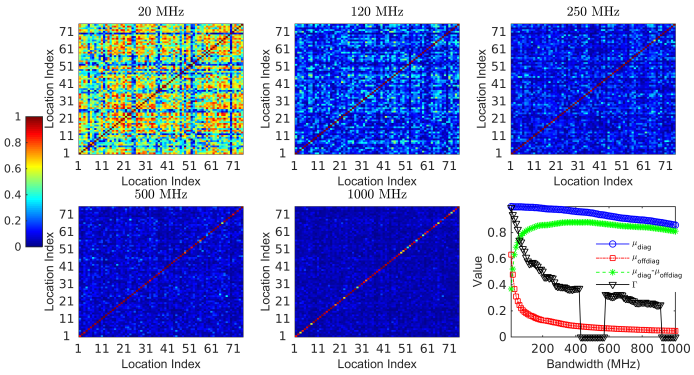


**Fig. 4**. Confusion matrix $\Phi$ under different bandwidths, and the statistics for bandwidths from 10 MHz to 1000 MHz with step size 10 MHz

## 5. CONCLUSION

In this paper, we propose WiFi-TRIPS and implement on USRPs to obtain CSIs from 802.11a/g/p transmission. To extend beyond the limitation of $10/20$ MHz bandwidth in 802.11a/g/p, we measure a total of 1 GHz bandwidth, from 4.9 GHz to 5.9 GHz. In the offline phase, the collected CSIs in 10 MHz bands are processed and concatenated into a 1 GHz fingerprints and stored into the database. In the online phase, the TR resonating strength is calculated using the stored fingerprints and the fingerprint from the unknown location, leading to the location estimation. Experiment results demonstrate the $5cm$ precision in an area of $20cm \times 70cm$ in a NLOS office environment with only one-link. The proposed method could be employed in commodity WiFi devices where multiple frequency bands are supported.

## 6. REFERENCES


[1] Z. Yang, Z. Zhou, and Y. Liu, "From RSSI to CSI: Indoor localization via channel response," *ACM Computing Surveys (CSUR)*, vol. 46, no. 2, pp. 25–1, 2013.

[2] M. Youssef and A. Agrawala, "The Horus WLAN location determination system," in *Proceedings of the 3rd International Conference on Mobile Systems, Applications, and Services*, New York, NY, USA, 2005, MobiSys '05, pp. 205–218, ACM.

[3] P. Bahl and V.N. Padmanabhan, "RADAR: an in-building RF-based user location and tracking system," in *Proc. IEEE INFOCOM*, 2000, vol. 2, pp. 775–784 vol.2.

[4] P. Prasithsangaree, P. Krishnamurthy, and P.K. Chrysanthis, "On indoor position location with wireless LANs," in *Personal, Indoor and Mobile Radio Communications, 2002. The 13th IEEE International Symposium on*, Sept 2002, vol. 2, pp. 720–724 vol.2.

[5] S. Sen, B. Radunovic, R.M. Choudhury, and T. Minka, "You are facing the Mona Lisa: Spot localization using PHY layer information," in *Proceedings of the 10th International Conference on Mobile Systems, Applications, and Services*, New York, NY, USA, 2012, MobiSys '12, pp. 183–196, ACM.

[6] J. Xiao, Wu K.S., Y. Yi, and L.M. Ni, "FIFS: Fine-grained indoor fingerprinting system," in *Computer Communications and Networks (ICCCN), 2012 21st International Conference on*, July 2012, pp. 1–7.

[7] Z. Wu, Y. Han, Y. Chen, and K.J. Ray Liu, "A time-reversal paradigm for indoor positioning system," *IEEE Trans. Veh. Commun.*, vol. 64, no. 4, pp. 1331–1339, April 2015.

[8] B. Wang, Y. Wu, F. Han, Y.H Yang, and K.J. Ray Liu, "Green wireless communications: A time-reversal paradigm," *IEEE J. Select. Areas Commun.*, vol. 29, no. 8, pp. 1698–1710, September 2011.

[9] B. Bloessl, M. Segata, C. Sommer, and F. Dressler, "An IEEE 802.11a/g/p OFDM Receiver for GNU Radio," in *ACM SIGCOMM 2013, 2nd ACM SIGCOMM Workshop of Software Radio Implementation Forum (SRIF 2013)*, Hong Kong, China, August 2013, pp. 9–16, ACM.

[10] "Ettus Research LLC," http://www.ettus.com/.

[11] "GNU Radio," http://gnuradio.org/.

[12] M. Speth, S.A. Fechtel, G. Fock, and H. Meyr, "Optimum receiver design for wireless broad-band systems using OFDM—Part I," *IEEE Trans. Commun.*, vol. 47, no. 11, pp. 1668 –1677, nov 1999.

[13] Tzi-Dar Chiueh and Pei-Yun Tsai, *OFDM Baseband Receiver Design for Wireless Communications*, John Wiley and Sons (Asia) Pte Ltd, 2007.

[14] M. Speth, S. Fechtel, G. Fock, and H. Meyr, "Optimum receiver design for OFDM-based broadband transmission II: A case study," *IEEE Trans. Commun.*, vol. 49, no. 4, pp. 571 –578, apr 2001.